

# COMPARISON OF GLR AND MAXIMAL INVARIANT DETECTORS UNDER STRUCTURED CLUTTER COVARIANCE

Hyung Soo Kim and Alfred O. Hero

Department of Electrical Engineering and Computer Science  
University of Michigan, Ann Arbor, MI 48109-2122  
Email: {kimhs,hero}@eecs.umich.edu

## ABSTRACT

There has been considerable recent interest in applying maximal invariant (MI) hypothesis testing as an alternative to the generalized likelihood ratio (GLR) test. This interest has been motivated by several attractive theoretical properties of MI tests including: exact robustness to variation of nuisance parameters, finite-sample min-max optimality (in some cases), and distributional robustness. However, in the deep hide target detection problem, there are regimes for which either of the MI and the GLR tests can outperform the other. We will discuss conditions under which the MI tests can be expected to outperform the GLR tests in the context of a radar imaging and target detection application. We will also show that the relative advantage of the MI tests is robust to boundary estimation errors.

## 1. INTRODUCTION

In [1], adaptive detection algorithms were developed for imaging radar targets in *structured* clutter by exploiting both the generalized likelihood ratio (GLR) principle and the invariance principle. In automatic target recognition, it is important to be able to reliably detect or classify a target in a manner which is robust to target and clutter variability yet maintains the highest possible discrimination capability. The GLR and invariance principles are worthwhile approaches since they often yield good constant false alarm rate (CFAR) tests.

A common assumption in homogeneous but uncertain clutter scenarios is that the target is of known form but unknown amplitude in Gaussian noise whose covariance matrix is totally unknown or *unstructured*. This assumption induces parameter uncertainty for which the general multivariate analysis of variance (GMANOVA) model [2] applies and optimal and suboptimal detection algorithms can be easily derived using the GLR principle [3]. However, when some structure on the covariance matrix is known a priori, improvements over this GLR test are possible. For adaptive arrays, Bose and Steinhardt [4] proposed an invariant detector which outperforms the Kelly's test [3] when the clutter covariance matrix is assumed to have a priori known block diagonal structure. In [1], the form of the GLR for block structured covariance is derived. Then the invariant approach considered in [4] is developed in the context of imaging radar for deep hide targets.

In this paper, the robustness properties of the GLR and maximal invariant (MI) tests derived in [1] are more closely investigated. Specifically, we show via simulation and experiment that

there are regimes of operation which separate the GLR and MI tests such as: target-to-clutter ratio, number of snapshots available, and prescribed false alarm level. We also show robustness with respect to boundary estimation errors and we determine minimum detectable target amplitude for a realistic SAR imaging application.

## 2. STRUCTURED GLR AND MI TESTS

Assume that the complex image has been scanned or reshaped into an  $m \times 1$  column vector  $\underline{x}$ . If multiple snapshots (chips)  $\underline{x}_1, \dots, \underline{x}_n$  of the terrain are available, they can be concatenated into a spatio-temporal matrix  $\mathbf{X}$  with columns  $\{\underline{x}_i\}_{i=1}^n$ . Let  $\underline{s}$  be the reshaped target vector to be detected in a clutter background  $\mathbf{N}$  having i.i.d. columns with zero mean. Then we have the simple image model

$$\mathbf{X} = a \underline{s} \underline{b}^H + \mathbf{N}$$

where  $a$  is an unknown target amplitude and  $\underline{b}^H$  accounts for the articulation of the target vector into the snapshot sequence, e.g. possible chip locations of the target. In spatially scanned radar images, the vector  $\underline{b}^H$  would be equal to  $[1, 0, \dots, 0]$  if the target presence is to be detected in the first image chip (1st column of  $\mathbf{X}$ ). In this case, this column will be called primary data while the rest of  $\mathbf{X}$  will be called secondary data. Also we assume that  $\mathbf{N}$  is a complex multivariate Gaussian matrix with i.i.d. columns:  $\text{vec}\{\mathbf{N}\} \sim \mathcal{CN}(\underline{0}, \mathbf{R} \otimes \mathbf{I}_n)$  where  $\underline{0}$  is an  $mn \times 1$  zero vector,  $\mathbf{I}_n$  is an  $n \times n$  identity matrix, and  $\otimes$  is the Kronecker product.

Under an assumption that the target straddles the known boundary of two independent regions, the spatial component has clutter covariance matrix  $\mathbf{R}$  which decomposes into a block diagonal matrix. Several cases, denoted in decreasing order of uncertainty as Cases 1, 2 and 3, of block diagonal covariance matrices are examined:

$$\mathbf{R} = \begin{bmatrix} \mathbf{R}_A & \mathbf{O} \\ \mathbf{O} & \mathbf{R}_B \end{bmatrix}$$

- Case 1:  $\mathbf{R}_A > 0, \mathbf{R}_B > 0$
- Case 2:  $\mathbf{R}_A > 0, \mathbf{R}_B = \sigma^2 \mathbf{I}$  where  $\sigma^2 > 0$
- Case 3:  $\mathbf{R}_A > 0, \mathbf{R}_B = \mathbf{I}$

where the subscripts denote the two different regions A and B. For real valued observations, the GLR method is shown to have explicit form for each of Cases 1, 2 and 3, involving the roots of a 4th order algebraic equation. For complex valued observations, 4th order algebraic equations for real and imaginary parts of the target

This work was supported in part by the Air Force Office of Scientific Research under MURI grant: F49620-97-0028.

amplitude  $a$  must be solved numerically. The maximal invariant statistics for Cases 1 and 2 were previously derived by Bose and Steinhardt and invariant tests were proposed based on these statistics in [4]. We treat Cases 1-3 in a unified framework and propose alternative MI tests which are better adapted to the deep hide target application.

GLR test statistics are listed in Table 1 where the measurement matrix is partitioned as

$$\mathbf{X} = \begin{bmatrix} \mathbf{X}_A \\ \mathbf{X}_B \end{bmatrix} = \begin{bmatrix} \underline{x}_{A1} & \mathbf{X}_{A2} \\ \underline{x}_{B1} & \mathbf{X}_{B2} \end{bmatrix}$$

and each column corresponds to pixel values in a different chip. The known target signature is  $\underline{s} = [\underline{s}_A^H \ \underline{s}_B^H]^H$ , and

$$p(a, \mathbf{X}_A) = (\underline{x}_{A1} - a\underline{s}_A)^H (\mathbf{X}_{A2} \mathbf{X}_{A2}^H)^{-1} (\underline{x}_{A1} - a\underline{s}_A)$$

$$q(a, \mathbf{X}_B) = \text{tr}\{(\mathbf{X}_B - a\underline{s}_B \underline{e}_1^T)^H (\mathbf{X}_B - a\underline{s}_B \underline{e}_1^T)\}.$$

Here  $\underline{x}_{A1}$  ( $m_A \times 1$ ) and  $\underline{x}_{B1}$  ( $m_B \times 1$ ) denote pixels in the chip which is being tested for containing the target where  $m_A + m_B = m$ . The MI tests are listed in Table 2 where

$$q_A = 1 + \underline{x}_{A1}^H (\mathbf{X}_{A2} \mathbf{X}_{A2}^H)^{-1} \underline{x}_{A1}, \quad v_2 = \frac{\text{tr}\{\mathbf{X}_B^H \mathbf{X}_B\}}{m_B}$$

$$q_B = 1 + \underline{x}_{B1}^H (\mathbf{X}_{B2} \mathbf{X}_{B2}^H)^{-1} \underline{x}_{B1}, \quad v_3 = n.$$

The complete derivations of the test statistics can be found in [5].

$\mathbf{R}_A$	$\mathbf{R}_B$	Log GLR: $\frac{1}{n} \ln \Lambda = \max_a \{ \cdot \}$
?	?	$\ln \frac{1+p(0, \mathbf{X}_A)}{1+p(a, \mathbf{X}_A)} + \ln \frac{1+p(0, \mathbf{X}_B)}{1+p(a, \mathbf{X}_B)}$
?	$\sigma^2 \mathbf{I}$	$\ln \frac{1+p(0, \mathbf{X}_A)}{1+p(a, \mathbf{X}_A)} + m_B \cdot \ln \frac{q(0, \mathbf{X}_B)}{q(a, \mathbf{X}_B)}$
?	$\mathbf{I}$	$\ln \frac{1+p(0, \mathbf{X}_A)}{1+p(a, \mathbf{X}_A)} + \frac{1}{n} [q(0, \mathbf{X}_B) - q(a, \mathbf{X}_B)]$

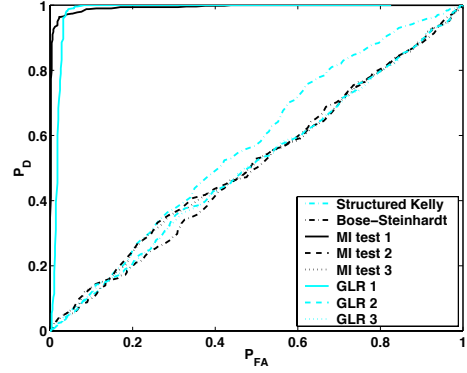
**Table 1.** GLR tests for Case 1, 2 and 3. (The notation ‘?’ denotes ‘unknown’ quantity in the model)

$\mathbf{R}_A$	$\mathbf{R}_B$	$\left[ \begin{bmatrix} \underline{s}_A^H & \underline{s}_B^H \\ \underline{s}_A^H & \underline{s}_B^H \end{bmatrix} \begin{bmatrix} \mathbf{K}_A & \mathbf{O} \\ \mathbf{O} & \mathbf{K}_B \end{bmatrix}^{-1} \begin{bmatrix} \underline{x}_{A1} \\ \underline{x}_{B1} \end{bmatrix} \right]^2$
?	?	$\mathbf{K}_A = q_A \mathbf{X}_{A2} \mathbf{X}_{A2}^H, \mathbf{K}_B = q_B \mathbf{X}_{B2} \mathbf{X}_{B2}^H$
?	$\sigma^2 \mathbf{I}$	$\mathbf{K}_A = q_A \mathbf{X}_{A2} \mathbf{X}_{A2}^H, \mathbf{K}_B = v_2 \mathbf{I}$
?	$\mathbf{I}$	$\mathbf{K}_A = q_A \mathbf{X}_{A2} \mathbf{X}_{A2}^H, \mathbf{K}_B = v_3 \mathbf{I}$

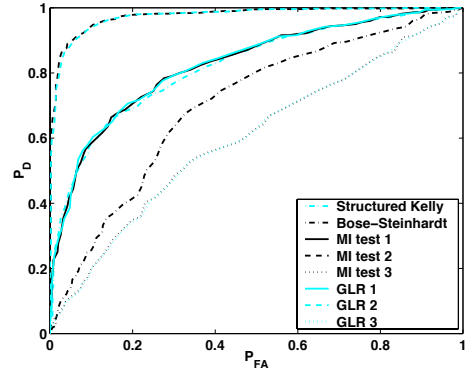
**Table 2.** MI tests for Case 1, 2 and 3

### 3. NUMERICAL COMPARISONS

To analyze the performance of the GLR and MI tests, ROC curves are generated and compared. In Fig. 1, the three GLR tests and the three MI tests matched to one of the three cases are compared. Also shown are ROC curves for structured Kelly’s test matched to Case 1, and Bose and Steinhardt’s test matched to Case 2. For each case, two tests stand out as significantly better than the other six: the GLR and MI tests which are matched to the underlying scenario.



(a) Case 1 (SNR = 19dB)



(b) Case 2 (SNR = 10dB)

**Fig. 1.** ROC curves for (a) Case 1 ( $m_A = 60, m_B = 40, n = 61$ ), and (b) Case 2 ( $m_A = 50, m_B = 50, n = 61$ ).

Of particular interest are the curve crossings in low  $P_{FA}$  regions between the GLR and the MI tests, and the relative advantages of those tests are more closely investigated in Fig. 2 and 3. In (a) of both figures, we increased  $n$  while fixing SNR. Note that the GLR and MI tests have ROCs which are virtually indistinguishable for large  $n$ . In (b), however, by increasing SNR while fixing  $n$ , the  $P_{FA}$  positions of the crossings of the ROCs for the GLR and MI tests decreased. In particular, if one fixes a level of false alarm, say  $P_{FA} = 0.1$ , then note from Fig. 2 (b) that the GLR test dominates the MI test for SNR = 19dB while the reverse is true for SNR = 7dB.

Since both the structured GLR and MI tests can only be implemented with the known boundary separating two different regions, sensitivity of the tests to boundary estimation errors is illustrated in Fig. 4. In both cases, ROC curves obtained with the biased boundary are compared with those using the true boundary. As can be seen, the overall performance of each test is degraded with false information, but the relative advantages of the GLR and MI tests still can be observed.

Next, we consider an application to real SAR imagery in Fig. 5. The image shown is a rural scene near Redstone Arsenal at

Huntsville, Alabama, reproduced from the data collected using the Sandia National Laboratories Twin Otter SAR sensor payload operating at X band (center frequency = 9.6 GHz, band width = 590 MHz). This clutter image consists of a forest canopy on top and a field on bottom, separated by a coarse boundary. The boundary was hand extracted and a  $9 \times 7$  SLICY target extracted from Fig. 6 (e) was inserted additively with the center at column 305 so that it straddles the boundary. The images in Fig. 6 correspond to the same target but viewed at different pose angles of azimuth. The data from which these images are reproduced was downloaded from the MSTAR SAR database at the Center for Imaging Science ([www.cis.jhu.edu](http://www.cis.jhu.edu)). From the realigned image in Fig. 7, we took subimages (chips) along the boundary by centering a  $20 \times 20$  window at the boundary and sliding it over the image from left to right. Each of these subimages is then concatenated into a column vector of size  $m = 400$  where  $m_A = 200$  and  $m_B = 200$ . Since we need at least 200 secondary chips to implement the structured detectors, clutter-alone pixels above and below those  $20 \times 20$  subimages taken along the boundary were used to generate enough secondary data for region A and B, respectively. Each of the subimages along the boundary was tested as a primary chip, and the test statistics derived under Case 1 were calculated and maximized over each possible location in the subimage. After normalizing the known target signature, we obtained the minimum magnitude of target amplitude required for each test to detect the target at the correct location. The resulting amplitude is the minimum detectable threshold for each of the detectors and these thresholds are shown in Table 3 for different number of secondary chips ( $n - 1$ ). As can be seen, with a large number of chips ( $n - 1 = 250$ ), both the GLR and MI tests perform as well as the structured Kelly's test. On the other hand, with a limited number of chips ( $n - 1 = 200$ ), MI test 1 successfully detects the target down to a significantly lower threshold than for GLR 1 and structured Kelly detectors.

Test	$ a $	
	$(n - 1 = 250)$	$(n - 1 = 200)$
MI test 1	$1.454 \times 10^{-2}$	$0.609 \times 10^{-1}$
GLR 1	$1.462 \times 10^{-2}$	$1.042 \times 10^{-1}$
Structured Kelly	$1.407 \times 10^{-2}$	$1.049 \times 10^{-1}$

**Table 3.** Minimum detectable amplitudes for detection of the target at the correct location.

As a final experiment we maximized the test statistics over the different target poses in Fig. 6 as well as over all possible locations along the boundary. Again the normalized signature from Fig. 6 (e) was inserted with  $|a| = 0.015$ , and 250 secondary chips were obtained from the surrounding clutter. Test values for the 3 detectors under Case 1 are obtained using 9 different target signatures. For each test the peak values for 9 target signatures are plotted in Fig. 8. Note that all the tests successfully picked the signature at the true pose and location for this target amplitude.

#### 4. CONCLUSION AND FUTURE RESEARCH

The deep hide scenario considered in this paper complicates the design of optimal target detectors. This scenario gives rise to block diagonal constraints imposed by the clutter covariance structure. Both GLR and MI tests can be derived under these constraints. Numerical results indicate that neither GLR nor MI tests dominate the other in terms of ROC performance. Both detectors have

comparable performance when high estimator accuracy is attainable, e.g. for a large number of independent clutter samples, but otherwise MI test is better especially in low  $P_{FA}$ . This property is also shown to be robust to segmentation errors. Therefore, MI test not only plays an important role as an alternative to the GLR procedure, but also has the desirable property of reliable performance in low  $P_{FA}$  with a small number of snapshots. The results in this paper are generalizable to other applications where invariance principle can be applied.

However, the known boundary assumption of the structured detectors may not be realistic in radar imaging applications. Thus, to move to a fully automatic procedure for combining boundary estimation and structured detection, image segmentation techniques such as the one in [6] should be investigated. In real applications, boundary estimation will be difficult even with a strong target straddling the boundary. Therefore, boundary estimation and its interaction with detection should also be investigated including sensitivity of detector performance to boundary estimations and tradeoffs between segmentation and detection.

#### 5. REFERENCES

- [1] H. S. Kim and A. O. Hero, "Adaptive target detection across a clutter boundary: GLR and maximally invariant detectors," *ICIP '00*, Vancouver, Canada, vol. 1, pp. 681-684, Sep. 2000.
- [2] T. Kariya and B. K. Sinha, *Robustness of Statistical Tests*, Academic Press, San Diego, 1989.
- [3] E. J. Kelly, "An adaptive detection algorithm," *IEEE Trans. Aerosp. Electron. Syst.*, vol. AES-22, pp. 115-127, Mar. 1986.
- [4] S. Bose and A. O. Steinhardt, "A maximal invariant framework for adaptive detection with structured and unstructured covariance matrices," *IEEE Trans. Sig. Proc.*, vol. 43, no. 9, pp. 2164-2175, Sep. 1995.
- [5] H. S. Kim and A. O. Hero, "Comparison of GLR and invariance methods applied to adaptive target detection in structured clutter," Tech. Rep. no. 323, Communications and Signal Processing Laboratory, University of Michigan, Nov. 2000.
- [6] I. Pollak, A. S. Wilsky and H. Krim, "Image segmentation and edge enhancement with stabilized inverse diffusion equations," *IEEE Trans. Image Proc.*, vol. 9, no. 2, pp. 256-266, Feb. 2000.

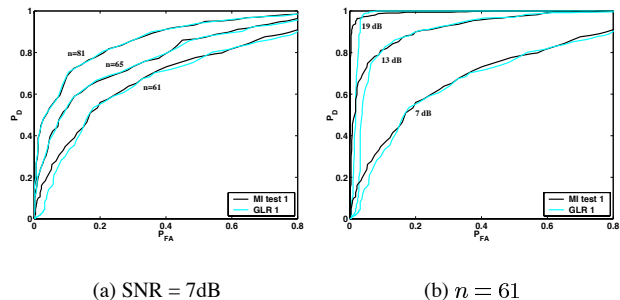


**Fig. 2.** Comparison of GLR and MI tests for Case 1 by (a) increasing  $n$  with fixed SNR and (b) increasing SNR with fixed  $n$  ( $m_A = 60, m_B = 40$ ).

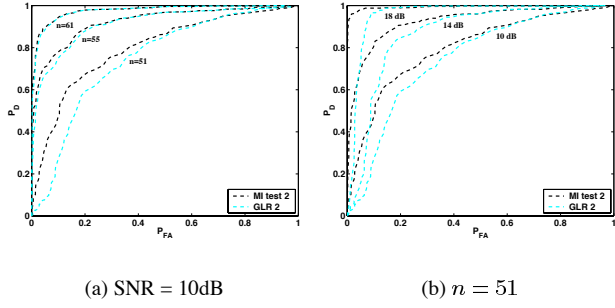


**Fig. 3.** Comparison of GLR and MI tests for Case 2 by (a) increasing  $n$  with fixed SNR and (b) increasing SNR with fixed  $n$  ( $m_A = 50, m_B = 50$ ).

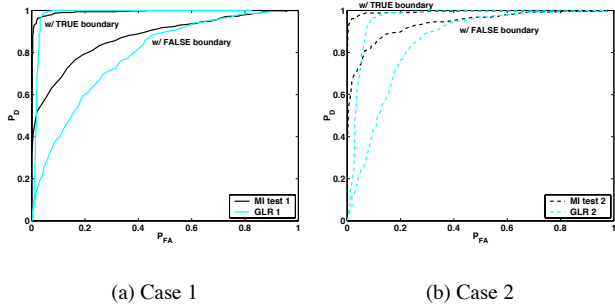


**Fig. 4.** Comparison of ROC curves using true boundaries and false boundaries (a) moved downward by one pixel and (b) moved upward by one pixel in each snapshot (True values: (a)  $m_A = 60, m_B = 40, n = 61$ , (b)  $m_A = 50, m_B = 50, n = 51$ ).

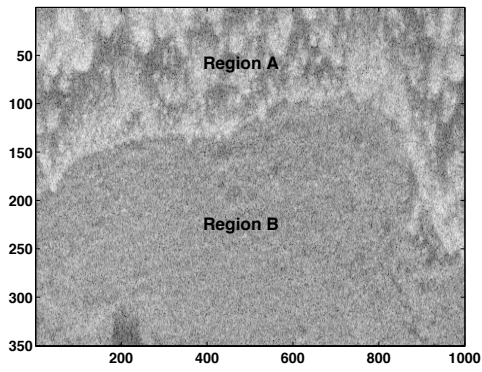


**Fig. 5.** SAR clutter image with target in Fig. 6 (e) straddling the boundary at column 305.

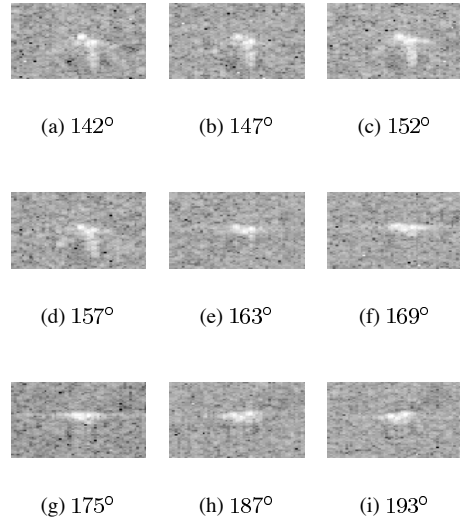


**Fig. 6.** SLICY canonical target images at elevation  $39^\circ$  and different azimuth angles. Image in (e) is inserted in Fig. 5.

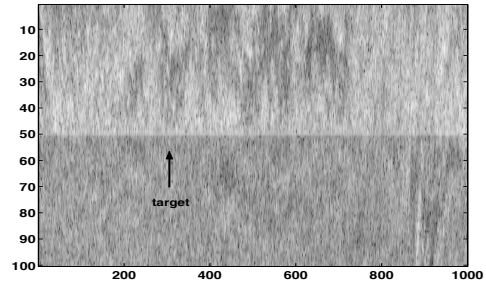


**Fig. 7.** Image realigned along the extracted boundary. SLICY target is located at column 305 with  $|a| = 0.015$ . This target is just above the minimal detectable threshold for the three tests investigated in Fig. 8.

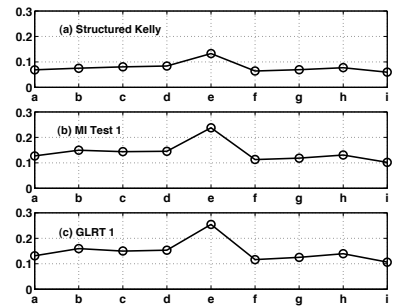


**Fig. 8.** Peak values obtained for 9 different target images in Fig. 6 ( $|a| = 0.015, n - 1 = 250$ ).